Acellular organ scaffolds for tumor tissue engineering

Anna Guller*[a, b, d], Inna Trusova[c], Elena Petersen[c], Anatoly Shekhter[b], Alexander Kurkov[b], Yi Qian[d], Andrei Zvyagin[a, e]

[a]Biofocus Research Centre, Macquarie University, 2109, New South Wales, Australia; [b]Sechenov First Moscow State Medical University, 8 Trubetskaya street, Moscow, 11992, Russia; [c]Moscow Institute of Physics and Technology, 9 Institutskiy per., Dolgoprudny, Moscow Region, 141700, Russia; [d]Faculty of Medicine and Health Science, Macquarie University, 2109, New South Wales, Australia; [e]Nizhny Novgorod State University, Russia.

ABSTRACT

Rationale: Tissue engineering (TE) is an emerging alternative approach to create models of human malignant tumors for experimental oncology, personalized medicine and drug discovery studies. Being the bottom-up strategy, TE provides an opportunity to control and explore the role of every component of the model system, including cellular populations, supportive scaffolds and signalling molecules.

Objectives: As an initial step to create a new ex vivo TE model of cancer, we optimized protocols to obtain organ-specific acellular matrices and evaluated their potential as TE scaffolds for culture of normal and tumor cells.

Methods and results: Effective decellularization of animals' kidneys, ureter, lungs, heart, and liver has been achieved by detergent-based processing. The obtained scaffolds demonstrated biocompatibility and growth-supporting potential in combination with normal (Vero, MDCK) and tumor cell lines (C26, B16). Acellular scaffolds and TE constructs have been characterized and compared with morphological methods.

Conclusions: The proposed methodology allows creation of sustainable 3D tumor TE constructs to explore the role of organ-specific cell-matrix interaction in tumorigenesis.

Keywords: tumor, tissue engineering, scaffold, decellularization, 3D cell culture in vitro.

1. INTRODUCTION

Recent advances in 3D cell and tissue culture emphasize the role of spatial microenvironment cues in the development of malignant tumors. In particular, this means that the commonly assumed understanding of tumor behaviour mechanisms and pharmacological screens for anti-tumor drugs verified on conventional 2D substrates could be misleading. Indeed, the luck of progress in a 5-year survival rate for the most spread types of cancer during the recent 30 years[1] as well as current 95% chances of falls in clinical trials of anti-neoplastic medicines[2] indicate the growing demand of biomimetic tumor models.

Tissue engineering, being initially a part of regenerative medicine focused on reconstruction of healthy tissues and organs for reconstructive surgery, now attracts great attention of the experimental oncologists as a very promising approach to create a bottom-up models of various types of cancer to dissect the intrinsic mechanisms involved into growth, progression, invasion and metastasis[3-9]. Tissue engineering constructs of tumors include tumor cells, 3-dimensional scaffold and a "3rd components" (other cell types, signalling molecules, physical factors etc.), with the intention to simulate tumor development and behaviour in dependence of the constituents of the microenvironment.

The biomimetic models of human diseases like cancer are in high demand for the development of novel diagnostics and therapy methods. These bioartificial tissues are ideal models for experimental science: 1) they demonstrate far more realistic physiological responses than Petri-dish-cultured cells, offering unprecedented reproducibility and outcomes acceptable to industry and regulators; 2) they do not require ethical approvals, and reduce animal testing and costs.

The purpose of this study was to evaluate feasibility of different approaches to development of acellular organ-specific scaffolds for tissue engineering of malignant tumors.

* *E-mail:* anna.guller@mq.edu.au

SPIE Micro+Nano Materials, Devices, and Systems, edited by Benjamin J. Eggleton, Stefano Palomba
Proc. of SPIE Vol. 9668, 96684G · © 2015 SPIE · CCC code: 0277-786X/15/$18 · doi: 10.1117/12.2202473

2. MATERIALS AND METHODS

2.1. Surgery and tissue collection

The study was performed in accordance with the ethics committee protocol for animal experiments of I.M. Sechenov First Moscow State Medical University. Two Chinchilla male rabbits of 3,000 ±120 g, being originally used for control observations in an unrelated surgical experiment, were anesthetized by injection of 40 mg/kg ketamine and 10 mg/kg xylazine intramuscularly (i/m) as a single dose and underwent bilateral nephrectomy with circumferential exposure and preservation of the adjacent parts of renal artery, renal vein and ureter (Fig. 1a). The excess perinephric fat was removed, and perihilum tissues were ligated. Intravenous catheter (26G, Flexicath, Apexmed, Netherlands) was inserted into the renal artery and secured with 6/0 Prolene suture to allow perfusion (Fig. 1 b). After that animals were euthanized by overdose i/m injection of ketamine. Prepared kidneys with inserted cannulas were extirpated, and the catheter was connected to a perfusion contour. Whole organ dissection of liver, lungs, heart and trachea was performed postmortem during 1 hour after the animal's death. The organs were immediately placed into cold sterile phosphate-buffered saline (PBS) (Gibco), containing 50 units/mL of sodium heparin (JSC "Synthez", Russia) until further operations (about 30 min). All the surgical procedures were performed under aseptic conditions.

2.2. Decellularization

The protocol A of whole kidney perfusion decellularization was adapted from[10]. Briefly, the cannula previously inserted into the renal artery of a rabbit's left kidney was connected to a perfusion contour of ORCA Bioreactor complex (Harvard Apparatus, USA) (Fig. 1 c), and the kidney was freely placed onto the bottom of the bioreactor organ chamber to allow continuous exposure to working solutions in closed fluid circulation setup (Fig. 1 d). The perfusion was initiated with PBS (Gibco), containing 50 units/mL of sodium heparin (JSC "Synthez", Russia) for 90 min. Then 0.1% sodium dodecyl sulfate (SDS) dissolved in sterile PBS has been perfused through native kidney vasculature for 16 hours with periodic changes for new portions of the medium at 1, 3, 6 and 12 hours of processing. Afterward, 1% SDS in PBS has been delivered to the organ during next 4 days with total replacement of the washing solution for fresh portions at every 6 hours. Finally kidneys of rabbits were perfused with 6 portions of sterile PBS (Gibco), containing 1% of antibiotic-antimycotic solution (Sigma Aldrich) and 2 mg/ml of ciprofloxacin for 2 days. The flow rate of perfusion was set at 30 ml/min for the whole experiment.

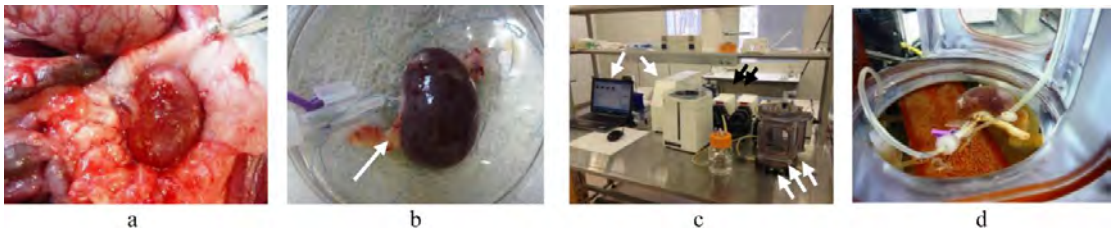

Figure 1. Preparation and start of decellularization of a rabbit left kidney (protocol A): (a) surgical approach; (b) cannula is secured in renal artery; arrow shows the ureter; (c) a view of ORCA bioreactor: a block of controller (single white arrows), a block of peristaltic pumps (double black arrows), and the organ chamber (triple white arrows); (d) a kidney in the organ chamber, the vasculature is connected to the perfusion contour.

The protocol B of immersion-agitation decellularization was applied to slices of rabbit right kidneys, fragments of livers, and to whole lungs, hearts and tracheas. Right kidneys first were perfused with heparinised PBS by a syringe. Fibrous capsules of right kidneys were carefully removed and the organs were cut transversely for disc slices of 3-6 mm in thickness. Each slice was immersed in an individual vial with 0.1% SDS solution in PBS. Livers were sectioned for fragments of the same thickness. Other dissected (but not cannulated) organs, including lungs, tracheas and hearts were transferred as a whole from heparinised PBS solution into individual containers with 0.1% SDS in PBS solution for further decellularization. The volume of the washing medium was approximately 10-20 times bigger than the volume of the samples. The organ containers were placed on digital speed control orbital shaker (OS-100, Joyfay International, China) and agitated at 120 revolutions per minute (rpm) for 12 hours. Then the concentration of SDS in the washing medium has been increased up to 1%, while the agitation rate was reduced to 90 rpm. Decellularization medium has been changed for fresh portions every 24 h until tissues became semi-transparent or transparent (3-6 days, depending on the organ). Following finishing of decellularization the organs and kidney slices were washed with sterile PBS (Gibco), containing 1% of antibiotic-antimycotic solution (Sigma Aldrich) and 2 mg/ml of ciprofloxacin for 2 days.

All the manipulations were performed at room temperature. During the decellularization the organs/ organ sections were photographed and sampled for morphological study. The scheme of the decellularization protocols and distribution of organ samples is depicted at Figure 2.

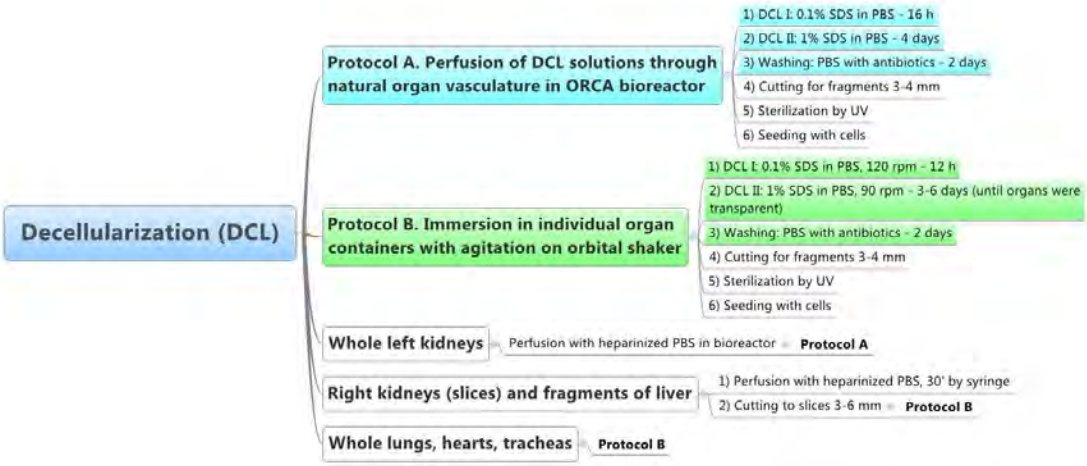

Figure 2. Overview of the decellularization and further processing of the tissues.

2.3. Recellularization of acellular organ scaffolds with linear cells

Preparation of scaffolds for cell seeding. After finishing of decellularization and washing, the small fragments (approximately 3×5 mm) of decellularized whole organs and the same size sectors of right kidney and liver slices were cut by a scalpel blade and put into 12-well flat bottom tissue culture plates (Corning, USA). One milliliter of sterile PBS with 1% antibiotic-antimycotic solution (Sigma Aldrich) was added to every well, and after that the decellularized tissue fragments were sterilized by ultraviolet light in a tissue culture hood for 3 hours. Then the tissues were aseptically transferred into sterile 50 ml tubes (Falcon) filled with DMEM/F12 culture medium supplemented with 10% fetal bovine serum, 2 mM L-glutamine, 100 U/ml penicillin/streptomycin, and 2 mg/ml ciprofloxacin and conditioned in a tissue culture incubator on a vertical rotary stage at 37 °C/ 6 rpm for 24 hours. After that the tissue fragments were placed into the individual wells of 12-well plate for further cell seeding. To define the quality of decellularization, the scaffolds were stained for DNA with Hoechst 33342 (1.0 μg/mL), a fluorescent nuclear dye.

Cell culture. Cells of Vero (African green monkey kidney, ATCC CCL81), MDCK (Madin-Darby canine kidney cells, ATCC CCL-34), C26 (murine-derived colon adenocarcinoma) and B16 (murine melanoma, ATCC CRL6322) cell lines were expanded by culture in DMEM/F12 supplemented with 10% fetal bovine serum, 2 mM L-glutamine, 100 U/ml penicillin/streptomycin under standard conditions (37 °C, humidified, 5% CO_2 gas atmosphere) during 7 days prior seeding on the scaffolds. The culture medium was changed every two days, and the cellular growth was controlled by phase contrast microscopy and cell counting. At the day of recellularization of scaffolds all the cells were stained with vital membrane cell tracer PKH26 (MINI26-1KT, Sigma Aldrich) for in vivo cell tracking.

Cell seeding and culture of tissue engineering constructs. Every scaffold prepared as described above was seeded with approximately 1×10^5 cells in 30 μl of DMEM/F12 supplemented with 10% fetal bovine serum, 2 mM L-glutamine, 100 U/ml penicillin/streptomycin. The cells were allowed to attach to the substrates for 1 hour in tissue culture incubator and then 2 ml of the culture medium was added to each well. Control scaffolds were left without cell seeding. Following that the tissue engineering constructs were cultured under standard conditions for 4 days. Growth medium was carefully changed once during this period without disturbing the constructs. A day after seeding and on a reference day 4 the constructs were imaged with phase contrast and fluorescence microscopy (for the last the samples were stained with Hoechst 33342 for DNA). After 4 days, control scaffolds and tissue engineering constructs were collected and fixed in 10% neutral buffered formalin for histological examination, in 70% ethanol for scanning electron microscopy and 2.5% buffered glutaraldehyde (at 4 °C) for semi-thin sectioning.

2.4. Morphology

2.4.1. Histological study

Formalin-fixed tissue samples were processed through alcohols of increasing concentrations and embedded in paraffin. Microtome slices of 5-6 μm in thickness were stained with hematoxylin and eosin (H&E), toluidine blue (for acid glycosaminoglycans), picrofuchsin by Van-Gieson (for collagen). The samples fixed in glutaraldehyde were post-fixed with 1% OsO_4 in cacodylate buffer for 1 h, dehydrated in graded alcohols, embedded in epoxy resin and cut using an ultra-microtome (LKB, Sweden) into semi-thin sections of 1-μm thickness, and then stained with methylene blue (azure II) basic fuchsine three chrome method (MAFT). Stained slides were mounted with Bio Mount HM mounting medium (Bio-Optica, Italy) and covered with cover slips. The H&E-stained and semi-thin histological preparations were examined by an upright light microscope Olympus BX51 using dry-air (4×/NA0.10; 10×/NA0.25;

20×/NA0.40) and oil-immersion (100×/NA1.25 oil) objectives (Olympus Optical, Japan) and photographed with a digital video camera SDU-252 (2048×1536 , "Spetsteletechnika", Russia).

2.4.2. Scanning electron microscopy (SEM)

The samples fixed in 70% ethanol were further dehydrated in 70-100% alcohols and underwent critical point drying in Emitech K850 Critical Point Dryer (Emitech Ltd., UK). Afterwards, the samples were mounted on stabs with conductive carbon/graphite paint (ProSciTech, Australia) and coated with gold using an Emitech K550 gold sputter coater (Emitech Ltd., UK). Electron microscope images were taken using a JEOL JSM- 6480 LA under accelerating voltage 5 kV, work distance 20 mm and size point 30 by the secondary electron imaging mode.

3. RESULTS AND DISCUSSION

3.1. Macroscopic observations

Significant macroscopic changes of organs have been revealed during the process of decellularization (Fig. 3). Despite the differences of rate of decellularization of the studied organs, progressive loss of natural color up to total discoloration, as well as various degree of volume reduction and increase of tissue transparency were visible in all the samples, as it was observed by many other researches[11-14]. Dense organs like heart and trachea show the slowest rate of these modifications.

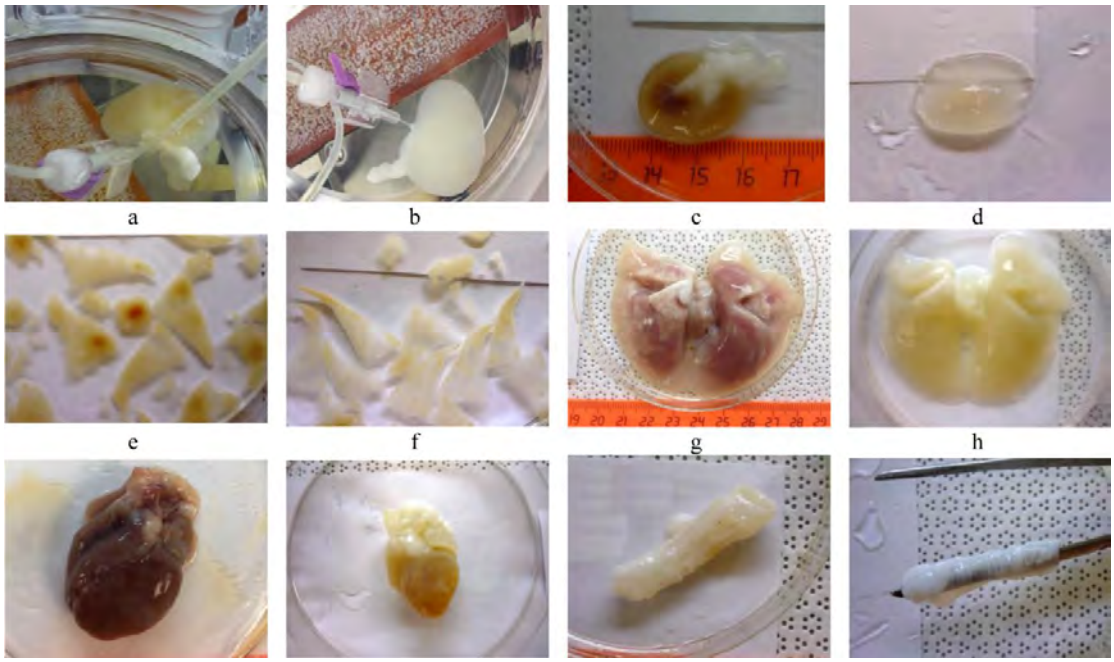

Figure 3. Effect of decellularization by protocols A (a, b) and B (c-l) on external appearance of organs and organ sections at certain time points of processing: (a, b) – left kidney, 12 h (a) and 3 days (b); (c, d) – a section of right kidney, 15 h (c) and 2 days (d); (e, f) – sections of liver, 15 h (e) and 24 h (f); (g, h) - whole lungs, 15 h (g) and 6 days (h); (i, j) - whole heart, 15 h and 6 days (j); (k, l) – whole trachea, 15 h (k) and 6 days (l). Note loss of natural color and increase of transparency.

In the samples of left kidneys processed by perfusion decellularization (the protocol A) the discoloration started from the hilum area and then spread to the rest part of the organ as marble-like pattern and later as diffuse semitransparency. The samples of whole lungs, processed by immersion-agitation (protocol B) demonstrated the spread of transparency from the outer margins to the central part of the organ. The same but less clear trend was notable in the samples of hearts and tracheas. The sections of liver and right kidneys became semitransparent faster than whole organs, but only the kidney matrix kept original shape of the slices, while the matrix of liver was significantly deformed and loosened.

3.2. Histological examination and SEM imaging of decellularized tissues

Histological examination and SEM imaging confirmed complete decellularization of kidney tissue by both studied protocols. The extracellular matrix of glomeruli as well as that of tubules generally preserved its spatial organization, but after immersion-agitation some deformation of tubules and flattening of the surfaces of glomeruli were visible (Fig. 4).Van-Gieson staining of decellularized kidneys signified that collagen carcass was not damaged, while toluidine blue staining indicated almost total loss of glycosaminoglycans. These observations are in accordance of the previously published results of detergent-based decellularization[15].

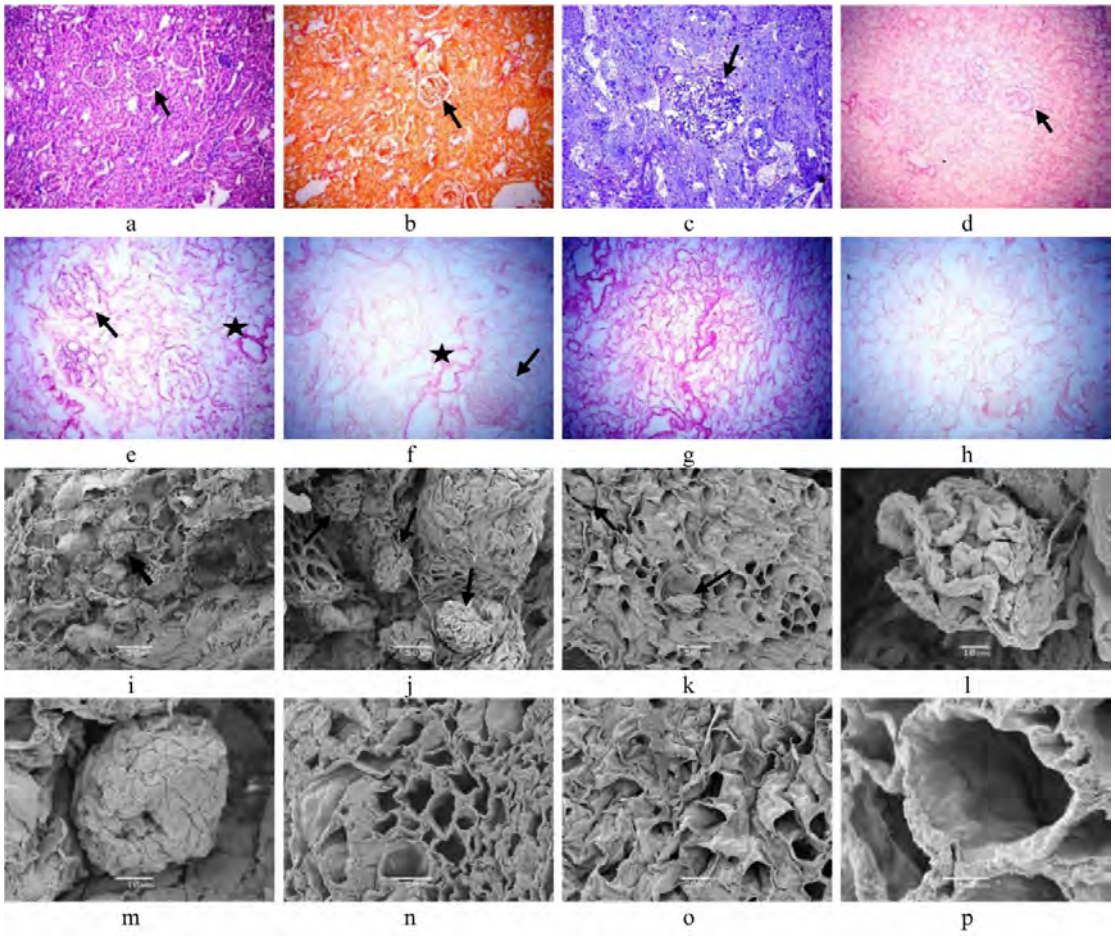

Figure 4. Effect of decellularization by the protocols A (d, e,g, j, l, and n) and B (f, h, k, m, o and p) on the kidney tissue: (a, b, c, i) – intact cortex of kidneys; note numerous glomeruli (arrows); (d-h) – histological images demonstrate absence of cells in kidney tissue after decellularization, well preserved stromal structure of glomeruli (arrows) and densification of perivascular matrix (stars) regardless the protocol; in addition, relative loosening of fibrous elements of stroma is visible in scaffolds treated by the protocol B, in comparison with the same components after the protocol A; (j-p) general stromal base of kidney cortex zone (j-m) with glomeruli (arrows) and medulla zone (n-p) is preserved after decellularization. The stromal structures after decellularization by the protocol B appear more flattened and deformed than after the protocol A treatment, but still preserve the key geometry features. Histological images, specimens stained with H&E (a, d-h), Van-Gieson's staining (b), c – semi-thin slice, MAFT. Original magnification: (a, b and d) - ×200; (c, e-h) - ×400. SEM images are presented at (i-p); scale bars: (i-k) – 50 µm; (l, m) – 10 µm; (n, o) – 20 µm; (p) – 5 µm.

Complete absence of cells as a result of immersion-agitation decellularization was also found in the samples of liver, lungs (including bronchial cartilage), ureters and renal arterial walls. In deep parts of heart tissue some basophilic material was visible implying the residual nuclear material, and in hyaline cartilage of trachea the areas containing well-shaped cell nuclei were revealed (Fig. 5). In contrast to notable decrease of metachromatic staining by toluidine blue indicating decrease in acid glycosaminoglycans, the spatial architecture and collagen content of the organ-specific extracellular matrix were kept in all the cases.

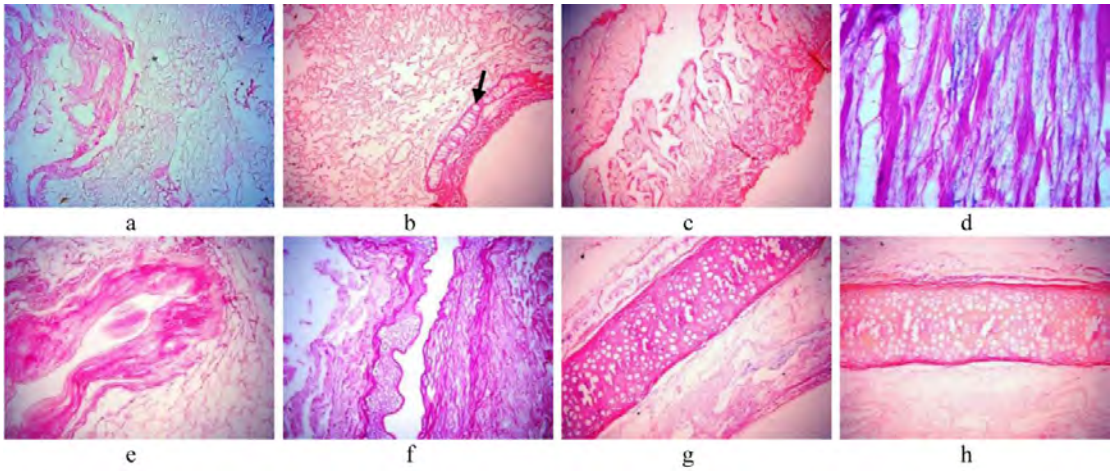

Figure 5. Effect of decellularization by the protocol B on the structure of (a) - liver sections; (b) – whole lungs; (c, d) whole heart (right atrium matrix is shown); (e) – ureter; (f) renal artery wall; (g, h) – whole trachea. Absence of any cellular material is notable in liver, lungs (including bronchial cartilage, arrow), ureter, and renal artery. Residual basophilic nuclear material is visible between fibrous bunds of myocardium (d) and numerous nuclei are revealed in trachea cartilage (g). Note also the well preserved fibrillary structure of collagen in perichondrium stained fuchsinophilic (h). Histological images, specimens stained with H&E (a, b, d-h) and Van-Gieson's stain (c, h). Original magnification: (a, f) - ×400; (b, c, e-h) - ×200; (d) - ×1000.

3.3. Results of recellularization of acellular organ-specific scaffolds

All the types of developed acellular organ-specific scaffolds were successfully repopulated by Vero, MDCK, C26 and B16 cells. Effective cellular adhesion on the matrices was confirmed by phase contrast and fluorescence microscopy at 24 hours after seeding, indicating absence of contact cytotoxicity of all the scaffolds and acceptability of the studied protocols of decellularization for further development of 3D culture models. Normal kidney cells (Vero, MDCK), in general, demonstrated lower rate of growth, in comparison with the cells of cancer cell lines (C26 and B16).

Preliminary analysis of cellular distribution in 4-days tissue engineering constructs show differences in spreading and penetration depth between Vero, C26 and B16 cells, growing on kidney acellular scaffold obtained by perfusion decellularization (Fig. 6). The number of colon carcinoma C26 and melanoma B16 cells attached to the scaffold surfaces was higher, than in tissue engineering construct with normal Vero cells, which probably reflects the difference in rates of proliferation or/and motility between cancer and normal cells. In addition, colon cancer cells demonstrated strong preference to grow in folders, grooves and cavities (see Fig. 6, e-g), while melanoma cells were mainly found on and near relatively flat matrix surfaces and along the decellularized vascular conduits. At the same time, probably to the differences in diameters, the smaller Vero and B16 cells penetrated narrow tubules on nephrons more deep and extensively, than C26 cells. The last were found on the internal surfaces of Bowman's membrane and on the loops of basal membranes of glomeruli. Interestingly, that many of C26 cells formed own matrix adhesions de novo as well as membrane blebbing (see Fig. 6 k). Membrane blebs are temporary plasma membrane protrusions, which are considered as functional response of a cell to reduced substrate adhesion[16]. This, in turn, emphasizes that acellular organ-specific scaffold provides a special type of 3D microenvironment, in contrast to conventional monolayer culture, where cells are gravity force-flattened and their contact substrate-contacting surface is much higher[17]. The observed blebbing, especially in single-sitting cells, can also be indirect evidence in favor of initiation of epithelial-mesenchymal transition, the key process for cancer invasion and metastasis[18].

The structure of matrices during the observation period has not been changed significantly, however, it appeared more blurry on the day 4, than initially. This may be a result of direct physical or chemical transformation of the scaffolds under the culture conditions as well as the effect of cell-mediated matrix remodeling implying cancer niche formation[19]. Further studies are needed to understand this mechanism better.

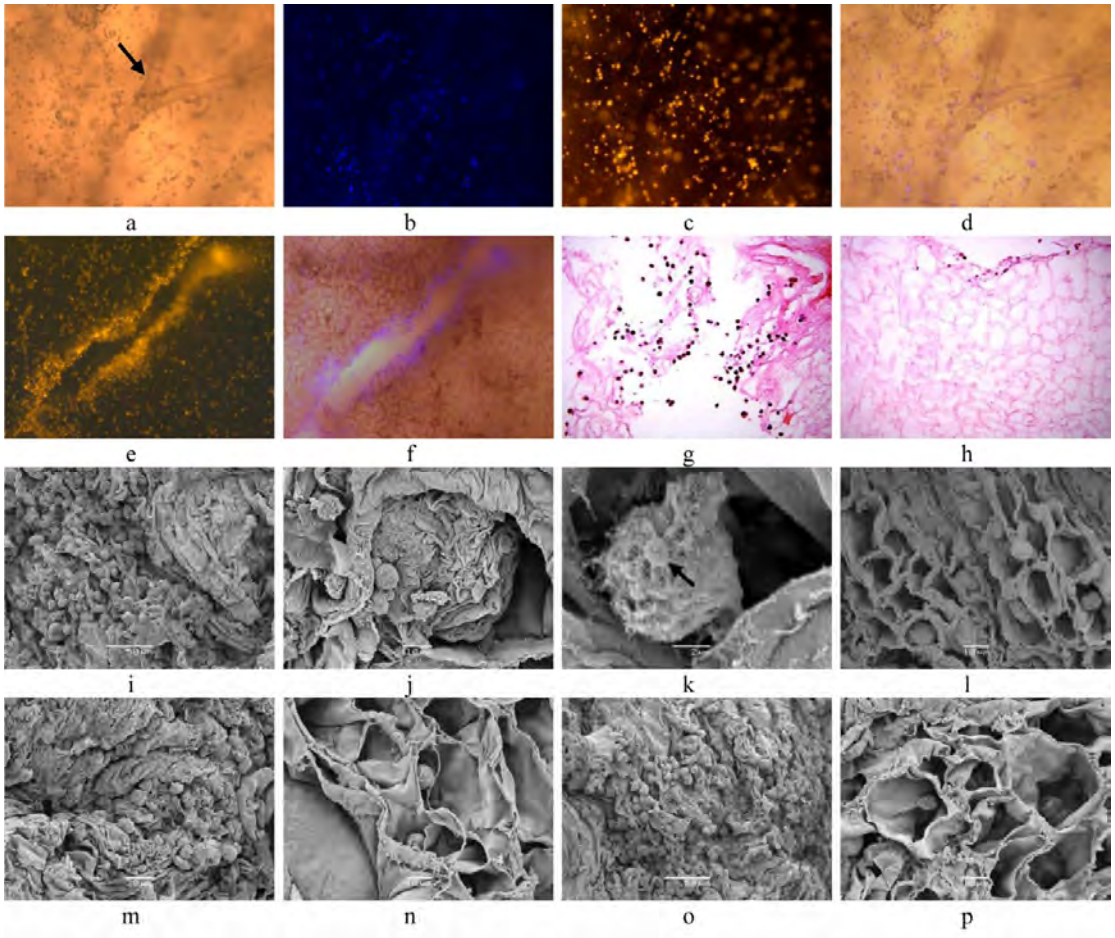

Figure 6. Recellularization of acellular kidney organ-specific matrix obtained by the protocol A: (a-d) - tissue engineering construct with Vero cells, ×10; phase contrast image demonstrating preservation of native vasculature (arrow) in the scaffold (a); Hoechst staining of nuclei (b), membrane tracer staining (c), overlay of phase contrast and Hoechst stained images (d); (e, f) – tissue engineering construct with C26 cells, ×10; membrane tracer staining of cells reveals dense cellular cluster, forming along a scaffold's groove (e), overlay of phase contrast and Hoechst stained image of the same area shows preservation of matrix of kidney tubules and some penetration of the cells into the volume of the scaffold (f); (g, h) - histological H&E stained images of tissue engineering constructs with C26 (g) and B16 (h) cells; note the difference in cellular numbers and distribution between the constructs depending on the cell types; original magnification ×400; (i-p) – SEM images of tissue engineering constructs with C26 (i-l), Vero (m, n) and B16 (o, p) cells. Cancer cells C26 and B16 demonstrate higher rate of the matrix surface repopulation (i, o), than normal kidney cells Vero (m). Penetration into renal tubules is relatively limited for large C26 cells (l), in contrast to Vero (n) and B16 (p) cells. Attachment of C26 cells to the Bowman's capsule matrix and a glomerulus surface (j); note blebbing of cell membrane (arrow) of a C26 cell and formation of cell-matrix adhesions (k). Scale bars in SEM images: (i, o) – 50 μm; (j, l, n, and p) – 10 μm; (k) – 2 μm; (m) – 20 μm.

4. CONCLUSION

This study was purposed to analyze the methodological aspects, possibilities and limitations of three-dimensional tumor modelling on acellular organ-specific scaffolds obtained by using of two strategies of tissue decellularization.

Acellular organ-specific scaffolds of kidneys were prepared in parallel by perfusion of the SDS solution through native organ vasculature and by immersion-agitation at 90 -120 rpm in the same detergent. Our data indicate that the method of delivery for decellularization agent can be neglected if the further use of whole-organ scaffold with internal vascular conduits is not expected. It seems, therefore, warranted to conclude that the immersion-agitation method of decellularization can be considered as a relatively high throughput alternative for development of organ-specific natural scaffolds for tissue engineering. However, a second conclusion that can be derived from the present investigation is that immersion-agitation decellularization can mechanically damage the spatial organization of matrix if applied to dissected fragments of organs instead of whole organs. At the same time we did not note any effect of this deformation on viability and adhesion of cells seeded on the scaffolds resulted from perfusion or immersion-agitation during the period of observation.

The current work has also shown the possibility to get whole-organ scaffolds from rabbit lungs and heart without perfusion, but by immersion-agitation method. This result and the procedure, to our knowledge, have not been published yet and indicate that complete or almost complete decellularization of such a big organs may be reached by a simplified approach of immersion-agitation, instead of perfusion in a bioreactor. In particular, this shows a possibility to use discarded human and animal organs, lacking of well-preserved vascular trees, for preparation of complex tissue engineering scaffolds.

Analysis of the results of recellularization of acellular organ-specific scaffolds obtained from rabbit organs confirms biocompatibility of the matrices, absence of contact cytotoxicity as it follows from successful 4-days culture of tissue engineering constructs. Four cell lines, including two normal kidney types (Vero and MDCK) and two tumor ones (C26 and B16) were integrated into the constructs with kidney, lungs, liver, trachea and heart matrices. Some signs of specific features of cancer behavior in colonization of matrices were revealed, like growth rate, preferable colonization sites, membrane blebbing associated with adhesions formation.

From the foregoing it seems reasonable to conclude that acellular organ-specific scaffolds can be produced from various types of organs and used for tumor tissue engineering. The immersion-agitation method of whole-organ decellularization can be considered a sustainable alternative to the perfusion decellularization for the purposes of 3D cell culture. The proposed approach may be used to develop novel biomimetic models to evaluate the effects of natural organ-specific microenvironment on cancer growth and progression.

ACKNOWLEDGEMENTS

Authors thank DRs Nicole Vella and Debra Birch (Macquarie University Microscopy Unit, Faculty of Science and Engineering) for their help with SEM, and Dr. Alexander Luzin (Sechenov First Moscow Medical University) for his guidance regarding the animal care procedures. The study was partially supported by the Russian Foundation for Basic Research (grants No 13-02-01363 and 13-04-12075) and by Grant of the Government of the Russian Federation for state support for scientific research under the guidance of leading scientists in Russian educational institutions of higher professional education, scientific establishments of the National Academy of Sciences and state research centers of the Russian Federation (Megagrant), No. 14.Z50.31.0022.

REFERENCES

[1] Williams, S. A., Anderson, W. C., Santaguida, M. T., et al., "Patient-derived xenografts, the cancer stem cell paradigm, and cancer pathobiology in the 21st century," Lab Invest, 93(9), 970-82 (2013).

[2] Hickman, J. A., Graeser, R., de Hoogt, R., et al., "Three-dimensional models of cancer for pharmacology and cancer cell biology: capturing tumor complexity in vitro/ex vivo," Biotechnol J, 9(9), 1115-28 (2014).

[3] Ingber, D. E., "Can cancer be reversed by engineering the tumor microenvironment?," Seminars in Cancer Biology, 18(5), 356-364 (2008).

[4] Hutmacher, D. W., Horch, R. E., Loessner, D., et al., "Translating tissue engineering technology platforms into cancer research," Journal of cellular and molecular medicine, 13(8a), 1417-1427 (2009).

[5] Burdett, E., Kasper, F. K., Mikos, A. G., et al., "Engineering tumors: a tissue engineering perspective in cancer biology," Tissue Eng Part B Rev, 16(3), 351-9 (2010).

[6] Ricci, C., Moroni, L., and Danti, S., "Cancer tissue engineering - new perspectives in understanding the biology of solid tumours - a critical review," OA Tissue Engineering, 1(1), 4 (2013).

[7] Fong, E. L., Santoro, M., Farach-Carson M. C., et al., "Tissue Engineering Perfusable Cancer Models," Curr Opin Chem Eng, 3, 112-117 (2014).

[8] Gill, B. J. and West, J. L., "Modeling the tumor extracellular matrix: Tissue engineering tools repurposed towards new frontiers in cancer biology," J Biomech, 47(9), 1969-78 (2014).

[9] Seib, F. P., Berry, J. E., Shiozawa, Y., et al., "Tissue engineering a surrogate niche for metastatic cancer cells," Biomaterials, 51, 313-9 (2015).

[10] Song, J. J., Guyette, J. P., Gilpin, S. E., et al., "Regeneration and experimental orthotopic transplantation of a bioengineered kidney," Nat Med, 19(5), 646-51 (2013).

[11] Park, K. M. and Woo, H. M., "Systemic Decellularization for Multi-organ Scaffolds in Rats," Transplantation Proceedings, 44(4), 1151-1154 (2012).

[12] Badylak, S. F., Weiss, D. J., Caplan, A., et al., "Engineered whole organs and complex tissues," Lancet, 379(9819), 943-52 (2012).

[13] Crapo, P. M., Gilbert, T. W. and Badylak, S. F., "An overview of tissue and whole organ decellularization processes," Biomaterials, 32(12), 3233-43 (2011).

[14] Maghsoudlou, P., Georgiades, F., Tyraskis A., et al., "Preservation of micro-architecture and angiogenic potential in a pulmonary acellular matrix obtained using intermittent intra-tracheal flow of detergent enzymatic treatment," Biomaterials, 34(28), 6638-48 (2013).

[15] Gilbert, T. W., Sellaro, T. L., and Badylak, S. F., "Decellularization of tissues and organs," Biomaterials, 27(19), 3675-83 (2006).

[16] Fackler, O. T., and Grosse, R., "Cell motility through plasma membrane blebbing," J Cell Biol, 181(6), 879-84 (2008).

[17] Baker, B. M. and Chen, C. S., "Deconstructing the third dimension: how 3D culture microenvironments alter cellular cues," J Cell Sci, 125(Pt 13), 3015-24 (2012).

[18] Kimlin, L. C., Casagrande, G., and Virador, V. M., "In vitro three-dimensional (3D) models in cancer research: an update," Mol Carcinog, 52(3), 167-82 (2013).

[19] Lu, P., Weaver, V. M. and Werb, Z., "The extracellular matrix: a dynamic niche in cancer progression," J Cell Biol, 196(4), 395-406 (2012).

PROCEEDINGS OF SPIE

Micro+Nano Materials, Devices, and Systems

Benjamin J. Eggleton
Stefano Palomba
Editors

6–9 December 2015
Sydney, Australia

Sponsored by
The University of Sydney (Australia)
CUDOS—An ARC Centre of Excellence (Australia)

Cosponsored by
NSW Government Trade and Investment (Australia)
AOS—The Australian Optical Society (Australia)
Office of Naval Research Global (United States)
U.S. Army Research, Development and Engineering Command (United States)

Published by
SPIE

Volume 9668

Proceedings of SPIE 0277-786X, V. 9668

SPIE is an international society advancing an interdisciplinary approach to the science and application of light.

SPIE Micro+Nano Materials, Devices, and Systems, edited by Benjamin J. Eggleton, Stefano Palomba
Proc. of SPIE Vol. 9668, 966801 · © 2015 SPIE · CCC code: 0277-786X/15/$18 · doi: 10.1117/12.2228503

The papers in this volume were part of the technical conference cited on the cover and title page. Papers were selected and subject to review by the editors and conference program committee. Some conference presentations may not be available for publication. Additional papers and presentation recordings may be available online in the SPIE Digital Library at SPIEDigitalLibrary.org.

The papers reflect the work and thoughts of the authors and are published herein as submitted. The publisher is not responsible for the validity of the information or for any outcomes resulting from reliance thereon.

Please use the following format to cite material from these proceedings:
Author(s), "Title of Paper," in *SPIE Micro+Nano Materials, Devices, and Systems*, edited by Benjamin J. Eggleton, Stefano Palomba, Proceedings of SPIE Vol. 9668 (SPIE, Bellingham, WA, 2015) Six-digit Article CID Number.

ISSN: 0277-786X
ISSN: 1996-756X (electronic)
ISBN: 9781628418903

Published by
SPIE
P.O. Box 10, Bellingham, Washington 98227-0010 USA
Telephone +1 360 676 3290 (Pacific Time)· Fax +1 360 647 1445
SPIE.org

Printed in the United States of America.

Publication of record for individual papers is online in the SPIE Digital Library.

SPIE. DIGITAL LIBRARY
SPIEDigitalLibrary.org

Paper Numbering: *Proceedings of SPIE* follow an e-First publication model. A unique citation identifier (CID) number is assigned to each article at the time of publication. Utilization of CIDs allows articles to be fully citable as soon as they are published online, and connects the same identifier to all online and print versions of the publication. SPIE uses a six-digit CID article numbering system structured as follows:

- The first four digits correspond to the SPIE volume number.
- The last two digits indicate publication order within the volume using a Base 36 numbering system employing both numerals and letters. These two-number sets start with 00, 01, 02, 03, 04, 05, 06, 07, 08, 09, 0A, 0B ... 0Z, followed by 10-1Z, 20-2Z, etc. The CID Number appears on each page of the manuscript.

Contents

PHOTONICS II

POSTER SESSION

Authors

Numbers in the index correspond to the last two digits of the six-digit citation identifier (CID) article numbering system used in Proceedings of SPIE. The first four digits reflect the volume number. Base 36 numbering is employed for the last two digits and indicates the order of articles within the volume. Numbers start with 00, 01, 02, 03, 04, 05, 06, 07, 08, 09, 0A, 0B...0Z, followed by 10-1Z, 20-2Z, etc.

Conference Committee

Conference Chair

Benjamin J. Eggleton, The University of Sydney (Australia)

Conference Co-chair

Stefano Palomba, The University of Sydney (Australia)

Conference Program Committee

Brian Abbey, La Trobe University (Australia)
Andrea M. Armani, The University of Southern California (United States)
Marcela M. M. Bilek, The University of Sydney (Australia)
Alvaro Casas Bedoya, The University of Sydney (Australia)
Peggy P. Y. Chan, RMIT University (Australia)
Wenlong Cheng, Monash University (Australia)
C. Martijn de Sterke, The University of Sydney (Australia)
James Friend, University of California, San Diego (United States)
Ewa M. Goldys, Macquarie University (Australia)
Daniel E. Gomez, Commonwealth Scientific and Industrial Research Organisation (Australia)
Min Gu, Swinburne University of Technology (Australia)
Stefan Harrer, IBM Research Collaboratory for Life Sciences-Melbourne (Australia)
Stephen Holler, Fordham University (United States)
Baohua Jia, Swinburne University of Technology (Australia)
Saulius Juodkazis, Swinburne University of Technology (Australia)
Adrian Keating, The University of Western Australia (Australia)
Dwayne D Kirk, Melbourne Center for Nanofabrication (Australia)
Alexander M. Korsunsky, University of Oxford (United Kingdom)
Zdenka Kuncic, The University of Sydney (Australia)
Gareth F. Moorhead, Commonwealth Scientific and Industrial Research Organisation (Australia)
David Moss, RMIT University (Australia)
Dragomir N. Neshev, The Australian National University (Australia)
Fiorenzo Gabriele Omenetto, Tufts University (United States)
Kostya Ostrikov, Commonwealth Scientific and Industrial Research Organisation (Australia)
Rupert F. Oulton, Imperial College London (United Kingdom)
Min Qiu, Zhejiang University (China)
David D. Sampson, The University of Western Australia (Australia)
Cather M. Simpson, The University of Auckland (New Zealand)

Volker J. Sorger, The George Washington University (United States)
Din Ping Tsai, Academia Sinica (Taiwan)
Niek F. Van Hulst, ICFO - Institut de Ciències Fotòniques (Spain)
Frédérique Vanholsbeeck, The University of Auckland (New Zealand)
Seok-Hyun Yun, Harvard Medical School (United States)
Yonggang Zhu, Commonwealth Scientific and Industrial Research Organisation (Australia)

Session Chairs

1A Nanostructured Materials I
Ann Roberts, The University of Melbourne (Australia)

1B Micro/Nanofluidics and Optofluidics I
Warwick P. Bowen, The University of Queensland (Australia)

1C Photonics I
Justin J. Cooper-White, The University of Queensland (Australia)

2A Nanostructured Materials II
Yuri S. Kivshar, The Australian National University (Australia)
Mikhail Lapine, University of Technology, Sydney (Australia)

2B Micro/Nanofluidics and Optofluidics II
Hywel Morgan, University of Southampton (United Kingdom)
Neetesh Singh, The University of Sydney (Australia)

2C Photonics II
Isabelle Staude, Friedrich-Schiller University (Germany)
Antony Orth, RMIT University (Australia)

3A Nanostructured Materials III
Frank Vollmer, Max-Planck-Institut für die Physik des Lichts (Germany)
Volker J. Sorger, The George Washington University (United States)

3B Nanophotonics for Biology and Medical Applications I
Krasimir Vasilev, University of South Australia (Australia)
Prineha Narang, California Institute of Technology (United States)

3C Photonics III
Igal Brener, Sandia National Labs (United States)
Christian Wolff, University of Technology, Sydney (Australia)

4A Nanostructured Materials IV
Kenneth B. Crozier, Harvard School of Engineering and Applied Sciences (United States)
Haisu Li, The University of Sydney (Australia)

4B Nanophotonics for Biology and Medical Applications II
Baohua Jia, Swinburne University of Technology (Australia)

4C Solar Cell Technologies
Diana Antonosyan, The Australian National University (Australia)
Alexander L. Gaeta, Columbia University (United States)

5A Biocompatible Materials I
Yuerui Lu, The Australian National University (Australia)
Sergey S. Kruk, The Australian National University (Australia)

5B Plasmonics I
Nikolai Strohfeldt, Universität Stuttgart (Germany)
Stefan A. Maier, Imperial College London (United Kingdom)

5C Fabrication I
Mingkai Liu, The Australian National University (Australia)
Arnan Mitchell, RMIT University (Australia)

6A Medical and Biological Micro/Nanodevices
Halina Rubinsztein-Dunlop, The University of Queensland (Australia)

6B Plasmonics II
Shaghik Atakaramians, The University of Sydney (Australia)
Timothy D. James, The University of Melbourne (Australia)

6C Fabrication II
David D. Sampson, The University of Western Australia (Australia)
Alexander S. Solntsev, The Australian National University (Australia)

7A Biocompatible Materials II
Peggy P. Chan, Swinburne University of Technology (Australia)

Introduction

In December 2013, the United Nations declared 2015 as the International Year of Light (IYL), recognizing the immense importance of light-based technologies in our lives, for our futures, and for the development of humankind.

In December 2015, the SPIE Micro+Nano Materials, Devices, and Applications symposium and the new Australian Institute for Nanoscience (AIN) at the University of Sydney's Camperdown campus offered the opportunity to celebrate the culmination of the IYL and heightened global awareness of the importance of light-based technologies, including nanoscience.

The SPIE symposium is an interdisciplinary forum for collaboration and learning among top researchers in all fields related to nano- and microscale materials and technologies. This 2015 event took place over 4 days, 6-9 December, and included both oral and poster presentations with a focus on nanostructured and biocompatible materials, medical and biological micro/nanodevices, micro/nanofluidics and optofluidics, nanophotonics for biology and medical applications, plasmonics, and solar cell technologies and fabrication.

The University of Sydney is Australia's first university with an outstanding global reputation for academic and research excellence. Located close to the heart of Australia's largest and most international city, the Camperdown campus features a mixture of iconic gothic-revival buildings and state-of-the-art teaching, research, and student support facilities. The University of Sydney attracts many of the most talented students in Australia drawn by its range of quality degrees and strong track record of research programs. The University's academics are leaders in their disciplines nationally and internationally, driving major research initiatives.

Sydney is Australia's truly international city and one of the world's most iconic and livable cities in the world, with plenty of open space, famous beaches, glittering harbour, waterways and bushland, great climate and vibrant culture rich of entertainment, cultural activities, and sporting events. Sydney is at the heart of Australia's economy, and is ranked first in the Asia Pacific in terms of intellectual capital and innovation. Sydney offers a safe and secure environment for individuals and families, with world-class health care, education, transport and telecommunications with a multicultural environment as over a third of Sydney's population was born overseas.

Benjamin J. Eggleton
Stefano Palomba